

**Supplementary Information for**

**New insights into the oxidation process from neutron and X-ray  
crystal structures of an O<sub>2</sub>-sensitive [NiFe]-hydrogenase**

Takeshi Hiromoto, Koji Nishikawa, Seiya Inoue, Hideaki Ogata, Yuta Hori, Katsuhiro Kusaka,  
Yu Hirano, Kazuo Kurihara, Yasuteru Shigeta, Taro Tamada, Yoshiki Higuchi

Authors for correspondence:

Taro Tamada, *Institute for Quantum Life Science, National Institutes for Quantum Science and Technology,  
4-9-1 Anagawa, Inage, Chiba 263-8555, Japan. Email: tamada.taro@qst.go.jp*

Yoshiki Higuchi, *Graduate School of Science, University of Hyogo, 3-2-1 Koto, Kamigori, Hyogo 678-1297,  
Japan. Email: hig@sci.u-hyogo.ac.jp*

***This PDF file includes:***

Supplementary text 1: Materials and methods.....	p. 2
Supplementary text 2: Results and discussion .....	p. 4
Figure S1 .....	p. 5
Figure S2 .....	p. 6
Figure S3 .....	p. 7
Figure S4 .....	p. 8
Figure S5 .....	p. 9
Figure S6 .....	p. 10
Table S1 .....	p. 11
Table S2 .....	p. 12
Table S3 .....	p. 13
Table S4 .....	p. 15
Table S5 .....	p. 17
Table S6 .....	p. 18
Table S7 .....	p. 19
ESI References.....	p. 20

## 1. Materials and methods

**Purification of DvMF-H<sub>2</sub>ase and preparation of its large crystal.** The cells of *Desulfovibrio vulgaris* Miyazaki F (DvMF) were cultured and harvested as described by Yahata *et al.*<sup>1</sup> In order to obtain the inactive oxidized enzymes, cell disruption was carried out by sonication under aerobic conditions, and the crude membrane pellet was recovered by centrifugation. The membrane-bound enzymes were solubilized from the pellet by digestion with trypsin (Sigma-Aldrich, St. Louis, MO, USA) and was subsequently purified as described previously.<sup>2</sup> Crystallization by macro-seeding was performed to obtain large single crystals. Crystallization mother liquor was prepared in heavy water (99.9% D<sub>2</sub>O; Cambridge Isotope Laboratories, Cambridge, UK) containing 0.2 mM enzyme, 30%(v/v) 2-methyl-2,4-pentane-d12-diol, 10 mM D-glucose-d12 and 25 mM Tris-d11-DCl (pD 7.4). A tiny seed crystal was immersed into 90  $\mu$ L of the mother liquor, which was then equilibrated at 283 K for six to eight weeks against a reservoir solution consisting of 40%(v/v) 2-methyl-2,4-pentanediol and 25 mM Tris-d11-DCl (pD 7.4) in D<sub>2</sub>O.

**Neutron diffraction experiments.** A resulting large crystal with dimensions of 1.8  $\times$  1.1  $\times$  0.7 mm<sup>3</sup> was mounted on a cryoloop and was cooled under a cold nitrogen-gas stream generated by a cooling device (Rigaku, Akishima, Japan).<sup>3</sup> Neutron diffraction from the crystal was measured at 100 K using the IBARAKI Biological Crystal Diffractometer (iBIX) equipped with 30 2D-detectors, which were based on ZnS scintillator screens coupled to a wavelength-shifting fiber-optic readout array,<sup>4</sup> at Materials and Life Science Experimental Facility (MLF) in Japan Photon Accelerator Research Complex (J-PARC), Tokai, Japan.<sup>5,6</sup> A full data set composed of a total of 24 frames of time-of-flight (TOF) data from different crystal orientations, each with an exposure time of 10.5 h, was collected, where the crystal was held static for each of the frames. Reduction of the TOF data was performed in the wavelength range of 3.0–5.8 Å using *STAR*Gazer,<sup>7,8</sup> resulting in the statistics listed in Table S1.

**X-ray diffraction experiments.** X-ray diffraction data were collected from the same crystal in preparation for joint X-ray and neutron (XN) refinement,<sup>3</sup> making it possible to compensate for the relatively low completeness and resolution of neutron data.<sup>9</sup> The data collection, covering a total rotation range of 180° as a continuous series of 0.5° oscillation images, was carried out on beamline BL26B1 at SPring-8, Harima, Japan, using a wavelength of 0.8000 Å. Anomalous scattering data were also collected over a total rotation range of 360° on beamline BL5A at Photon Factory (PF), Tsukuba, Japan, using two wavelengths near the X-ray absorption K-edge of nickel (1.4879 Å). All data sets were indexed, integrated, and scaled with the program package *XDS*,<sup>10</sup> and their statistics are summarized in Table S1.

**Structure determination and refinement.** Initial phases for the X-ray data at 1.04 Å resolution were calculated by maximum-likelihood molecular replacement with the program *Phaser*,<sup>11</sup> implemented in the *PHENIX* system.<sup>12</sup> After several rounds of the iterative manual rebuilding of protein and water coordinates, the active site binuclear complex and the three Fe–S clusters were constructed based on 2mFo–DFc and mFo–DFc electron-density maps. The model building and the water picking were conducted using *Coot*.<sup>13</sup> The X-ray coordinates were then obtained through the respective refinements of the occupancy for alternative conformations and the anisotropic displacement parameters for protein coordinates. One Mg<sup>2+</sup> ion and one Cl<sup>-</sup> ion were identified based on their interatomic distances to the respective surrounding atoms. Also, it was indicated from the anomalous scattering data that a part of Ni ion in the Ni–Fe complex was released and newly formed a square-planer complex at the active site. In order to estimate the *B*-factors of each Ni site, their occupancies were calculated as a total of 100% using the program *phenix.refine* in *PHENIX*,<sup>12</sup> giving one site with an occupancy of 68% and a *B*-factor of 9.6 Å<sup>2</sup> and the other one with an occupancy of 32% and a *B*-factor of 10.4 Å<sup>2</sup>. By subsequently considering the *B*-factor of 9.6 Å<sup>2</sup> for the main Ni site, the occupancy of a monooxygen species at the bridging ligand site was estimated as 100%, as indicated in Table S2. The statistics for the structure refinement are given in Table S1.

The X-ray coordinates obtained above were used for joint XN refinement with the program *phenix.refine* in *PHENIX*.<sup>12</sup> After an initial rigid-body minimization, hydrogen (H) atoms were

introduced to all unexchangeable sites in the protein model, and deuterium (D) atoms to the remaining exchangeable sites except for water molecules. Maximum-likelihood-based refinement of individual coordinates was then performed, followed by the refinement of isotropic displacement parameters for the H and D atoms. Deuterium for D<sub>2</sub>O were further generated according to their positive peaks on a mFo–DFc neutron scattering length density map at this refinement stage, with manual adjustment of their orientations. Following several cycles of refinement, the protonated forms of dissociative functional groups were assigned by detailed analyses using mFo–DFc H/D-omit neutron scattering length density maps. Finally, the H/D occupancies of all exchangeable sites over the protein were estimated, and their isotropic *B*-factors were refined. The joint XN refinement converged to crystallographic  $R_{\text{work}}/R_{\text{free}}$  values of 18.9/22.0% for the neutron data and of 14.3/14.8% for the X-ray data. The final coordinates comprise 14,708 protein atoms, including 7,858 hydrogen (H) and deuterium (D) atoms. The mean *B*-factor values are 14.8 Å<sup>2</sup> for the protein-constituting atoms, 13.0 Å<sup>2</sup> for the main-chain atoms and 15.3 Å<sup>2</sup> for the side-chain atoms. A total of 842 heavy water molecules were assigned through X-ray structure refinement at 1.04 Å. Of these, 727 waters were interpreted as full D<sub>2</sub>O molecules by their apparent neutron scattering length density distributions for deuterium. One of the D<sub>2</sub>O molecules identified in the protein interior was assigned as having two different orientations because of its particularly large positive density (Fig. S4b). The remaining 115 waters with alternative positions were assigned as single O atoms. The mean *B*-factor value for the water molecules, including D atoms, was calculated as 32.4 Å<sup>2</sup>. The refinement statistics are summarized in Table S1.

**Quantum chemical calculations.** There are sophisticated methods for determining geometrical structures by combining experimental and calculated data.<sup>14</sup> Herein, the root-mean-square deviations (RMSDs) of each optimized structure from our obtained crystal structure were then calculated to compare the calculated structures and the experimental data, because many chemical species, charges, and spin states were considered to determine the appropriate geometrical and electronic structures. All calculations were performed using the density functional theory (DFT) with the B3LYP functional and 6-31G\* basis set,<sup>15–17</sup> implemented in the Gaussian 16 program package.<sup>18</sup> Calculation models were derived from our obtained crystal structure by extracting the active site coordinates including the Ni/Fe centers, one CO, two CN<sup>-</sup>, the bridging species (X or Sy–X), four cysteines (Cys81<sup>L</sup>, Cys84<sup>L</sup>, Cys546<sup>L</sup>, and Cys549<sup>L</sup>) and one glutamate (Glu34<sup>L</sup>) as shown in Figs. 2b and 2d in the main text. Then, we constructed the cluster models changed in the Ni charges (Ni<sup>2+</sup> or Ni<sup>3+</sup>), the spin states (high or low spin), and the bridging species (O<sup>2-</sup>/OH<sup>-</sup> or Sy–O<sup>-</sup>/Sy–OH) between the Ni/Fe centers, in which the oxidation state of Fe<sup>2+</sup> was assumed through the calculations. Terminal carbon atoms of all residues in the optimized structures (Cartesian coordinates) were fixed during the geometrical optimizations. The Cartesian coordinates identified by quantum chemical calculations are shown in Fig. S2a for Ni-B and in Fig. S2b for the square-planer Ni complex bridged by a cysteine sulfenate ligand, respectively.

## 2. Supplementary Results and discussion

**Observation of the H/D atoms involved in potential proton transfer pathways.** At the branching point for three putative pathways for proton transfer (Fig. S4a), O $\epsilon$ 2 (Glu16<sup>L</sup>) interacts with two water molecules and the doubly protonated imidazole ring of His36<sup>L</sup> (Fig. S4c).<sup>19,20</sup> The relatively long distance of 2.94 Å between the proton of N $\epsilon$ 2 (His36<sup>L</sup>) and O $\epsilon$ 2 (Glu16<sup>L</sup>) suggests an electrostatic interaction, rather than a hydrogen bond. His36<sup>L</sup> is connected to Arg38<sup>L</sup> located at the protein surface *via* hydrogen bonds with Asp28<sup>L</sup> and two water molecules, designated as Path 1 (Fig. S4a). Another hydrogen-bonding network leading to the Mg<sup>2+</sup>-binding site comprises His522<sup>L</sup>, Glu62<sup>L</sup>, and five water molecules (Path 3). In contrast, Path 2 leads to Tyr44<sup>S</sup> exposed to the bulk solvent *via* hydrogen bonds with Glu46<sup>S</sup> and two water molecules. All the protons of water molecules involved in the hydrogen-bonding networks are largely exchanged by deuterium, making it possible to determine their correct orientations. Of these water molecules, only one (W842), located in the vicinity of the carboxylate group of Glu46<sup>S</sup> in Path 2, shows a particularly large positive density comparing to that of the adjacent water molecule (W83) (Fig. S4b). This implies that the single D<sub>2</sub>O molecule adopts another orientation in response to the surrounding environment. The O $\epsilon$ 2 (Glu46<sup>S</sup>) is associated with the O $\eta$  (Tyr44<sup>S</sup>) by a relatively short distance of 2.58 Å (Fig. S4c), but the neutron scattering length density distribution in the hydrogen bond between O $\epsilon$ 2 (Glu46<sup>S</sup>) and O $\eta$  (Tyr44<sup>S</sup>) indicates that a D atom is attached to O $\eta$  (Tyr44<sup>S</sup>). Of the three possible transfer pathways, only Path 2 has short hydrogen bonds. Unusually short hydrogen bonds can be involved in proton transfer reactions.<sup>21</sup> Based on these structural features of DvMF-H<sub>2</sub>ase determined by neutron diffraction, the protons produced and liberated by H<sub>2</sub> oxidation reaction at the active site probably migrate through Path 2, as proposed originally for the O<sub>2</sub>-sensitive *Desulfovibrio gigas* (Dg) [NiFe]-H<sub>2</sub>ase.<sup>22</sup>

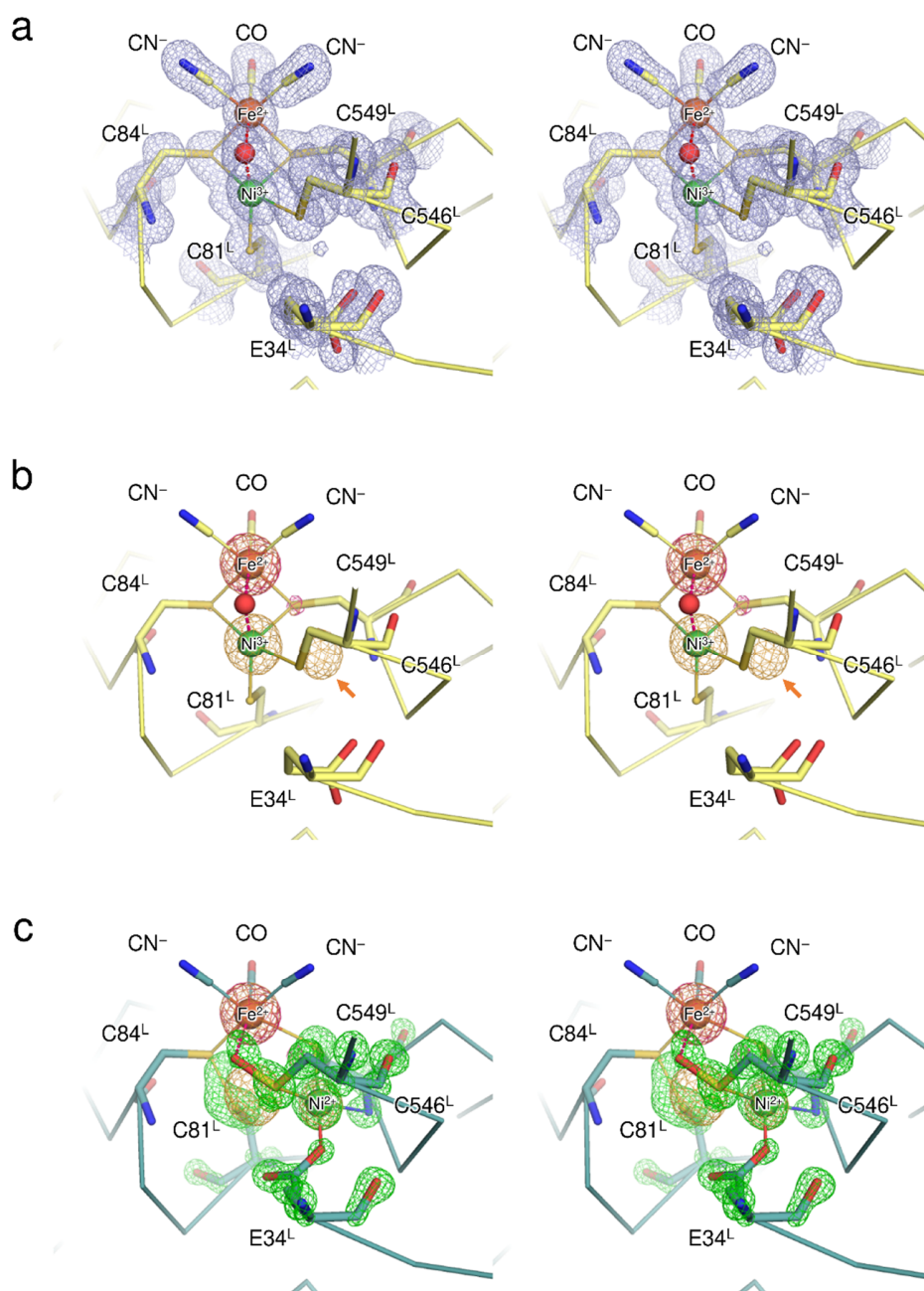


**Figure S1** (a) Stereo view of Fig. 2a in the main text. (b) Stereo view of the Ni–Fe complex in Ni-B, superimposed with model-phased anomalous difference Fourier maps at wavelengths of 1.4800 Å (contoured at 4.0σ, bright orange mesh) and 1.4900 Å (contoured at 5.0σ, hot pink mesh). A surplus peak derived from nickel was found adjacent to the Ni site of Ni-B, as indicated by an orange arrow. (c) Stereo view of Fig. 2c in the main text.

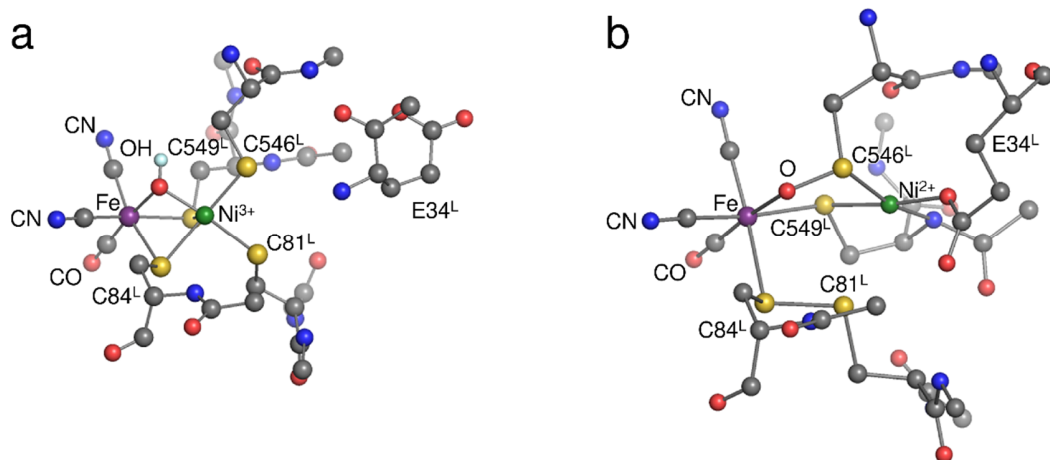


**Figure S2** (a) Optimized structure identified by DFT calculations based on the active site complex in Ni-B. The atomic coordinates are listed in Table S3. Color coding: H, pale cyan; C, gray; N, blue; O, red; S, yellow; Fe, purple; Ni, green. (b) Optimized structure identified by DFT calculations based on the square-planer Ni complex. The atomic coordinates are listed in Table S4.

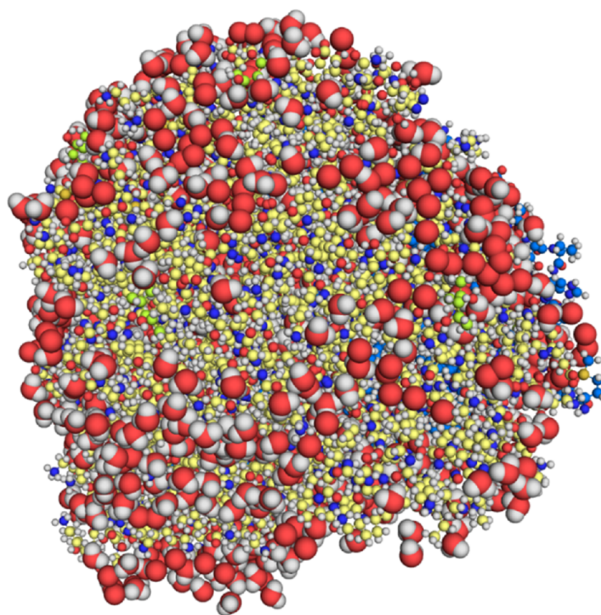


**Figure S3** Neutron structure of DvMF-H<sub>2</sub>ase. The protein structure is drawn as balls and sticks. Water molecules are shown as red spheres. Both H and D atoms are colored white.

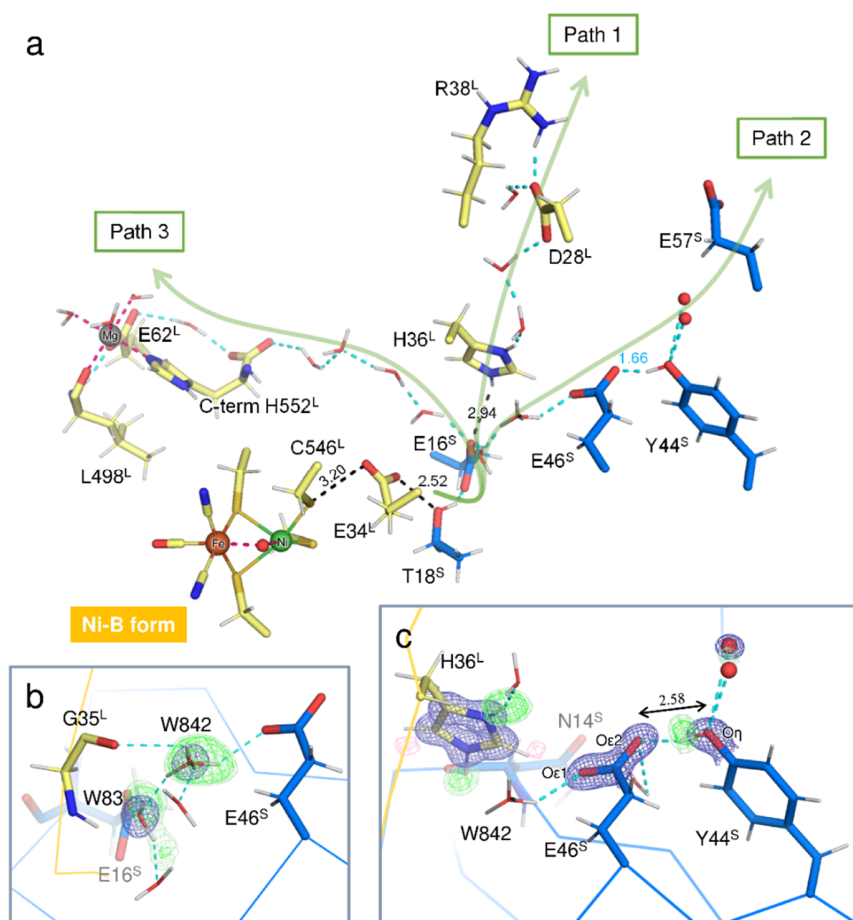


**Figure S4** Proposed pathways for proton transfer in DvMF-H<sub>2</sub>ase. (a) Three candidate pathways starting from Glu34<sup>L</sup> are indicated with pale green arrows and are labeled as Path 1, Path 2, and Path 3.<sup>19</sup> Hydrogen bonds are depicted by cyan dashed lines, where the oxygen–oxygen (O–O) and nitrogen–oxygen (N–O) distances are between 2.6 Å and 3.2 Å. The doubly protonated His36<sup>L</sup>-imidazole Nε2 atom points away from the Glu16<sup>L</sup> carboxylate group at a distance of 3.43 Å, and its electrostatic interaction is shown as a black dashed line. Potential hydrogen bonds occurring during catalytic H<sub>2</sub> oxidation are also indicated by black dashed lines. Amino-acid residues and solvent molecules involved in these hydrogen bonds are represented by sticks. One water molecule interacting with Tyr44<sup>S</sup> occupies two alternative positions, shown as red spheres. (b) Close-up view of a D<sub>2</sub>O molecule (W842) interacting with Glu46<sup>S</sup>, superimposed with a 2mFo–DFc electron-density map (contoured at 2.0σ, blue mesh) for selected waters (W842 and W83) and with their mFo–DFc H/D-omit neutron scattering length density maps (contoured at 3.2σ and 2.8σ, colored green and pale green, respectively). The water protons of W842 with an orientation are shown as white sticks, and that with an alternative orientation are as gray sticks. (c) Close-up view of a short hydrogen bond between Glu46<sup>S</sup> and Tyr44<sup>S</sup>, superimposed with a 2mFo–DFc electron-density map and with mFo–DFc H/D-omit neutron scattering length density maps in the same way as in (b). The negative neutron scattering length densities for H at –2.8σ are shown as pink mesh.

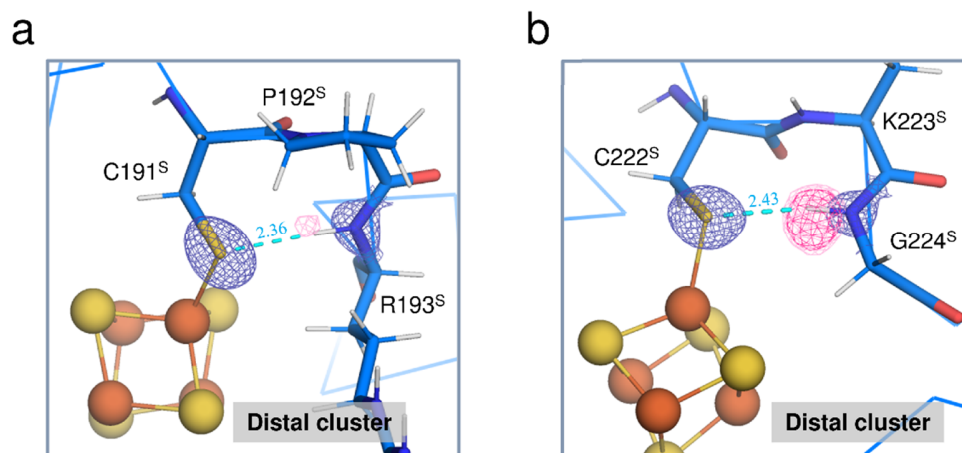


**Figure S5** Hydrogen bonds (a) between the main-chain amide N (Arg193<sup>S</sup>) and Sy (Cys191<sup>S</sup>) and (c) between N (Gly224<sup>S</sup>) and Sy (Cys222<sup>S</sup>). The 2mFo–DFc electron-density maps (contoured at 2.0 $\sigma$ ) for the amide N and the thiolate Sy atoms are represented as blue mesh. Their mFo–DFc H/D-omit neutron scattering length density maps were calculated for visualizing the H and D positions and were superimposed on each atom pair, where the negative peaks at  $-3.2\sigma$  and  $-2.8\sigma$  are colored hot pink and pink, respectively. The interatomic distance between N (Arg193<sup>S</sup>) and Sy (Cys191<sup>S</sup>) is 3.37 Å and that between N (Gly224<sup>S</sup>) and Sy (Cys222<sup>S</sup>) is 3.44 Å.

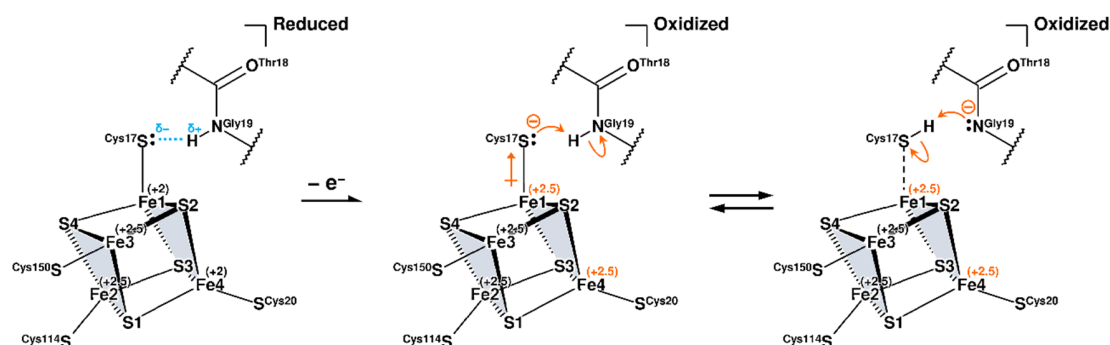


**Figure S6** Proposed reaction for one-electron oxidation at the proximal cluster. The proximal cluster in its reduced state (*left*) can be divided into two subclusters (shaded by pale gray),<sup>22</sup> Fe1-S2-Fe4-S3 and Fe2-S1-Fe3-S4, where each subcluster is bridged by four internal Fe–S bonds that are shorter than the other eight bonds as seen in Fig. 5 in the main text. One subcluster containing a ferrous pair provides one electron that is transferred to the protein surface *via* the other clusters in the catalytic H<sub>2</sub> oxidation,<sup>24</sup> resulting in the oxidized [4Fe-4S]<sup>2+</sup> cluster comprised of two Fe<sup>2.5+</sup>-Fe<sup>2.5+</sup> delocalized pairs (*center* and *right*). Increasing the charge at the subcluster may enhance the polarization of the Fe1–Sy (Cys17<sup>S</sup>) coordination bond, leading to the abstraction of the Gly19<sup>S</sup> amide proton (*center*); however, the protonation at the Cys17<sup>S</sup> Sy atom can cause the instability of the coordination to Fe1 (*right*). Presumably, the proton delocalization between the two oxidized states takes place to maintain the Fe1–Sy (Cys17<sup>S</sup>) coordination bond as observed in this study.

**Table S1. Data collection and refinement statistics**

	Neutron	X-ray	Anomalous-1	Anomalous-2
<i>Data collection</i>				
Beam source	iBIX (J-PARC/MLF)	BL26B1 (SPring-8)	BL5A (PF)	BL5A (PF)
Wavelength (Å)	3.0–5.8	0.8000	1.4800	1.4900
Space group	<i>P</i> 2 <sub>1</sub> 2 <sub>1</sub> 2 <sub>1</sub>			
Cell dimensions				
<i>a</i> , <i>b</i> , <i>c</i> (Å)	66.6, 98.5, 126.8	66.7, 98.5, 126.9	66.7, 98.5, 126.9	66.7, 98.5, 126.9
Resolution (Å)	20–2.20 (2.32–2.20)	50–1.04 (1.07–1.04)	50–1.50 (1.53–1.50)	50–1.50 (1.53–1.50)
Unique reflections	38,335	397,623	256,471	256,153
<i>R</i> <sub>merge</sub> <sup>‡</sup> (%)	22.0 (39.4)	5.9 (46.1)	6.2 (19.3)	6.8 (21.0)
<i>R</i> <sub>meas</sub> (%)	26.6 (47.3)	6.2 (49.6)	6.8 (21.2)	7.4 (23.1)
CC <sub>1/2</sub>	0.92 (0.57)	100 (92.4)	99.6 (95.9)	99.4 (95.4)
< <i>I</i> /σ( <i>I</i> )>	4.9 (2.3)	19.7 (4.1)	33.2 (5.8)	32.5 (5.0)
Completeness (%)	90.1 (93.5)	99.9 (99.6)	99.2 (97.5)	99.1 (96.3)
Redundancy	2.6 (2.8)	8.5 (7.2)	6.5 (6.1)	6.4 (5.7)
<i>Refinement</i>				
Used resolution (Å)	20–2.20 (2.25–2.20)	50–1.04 (1.05–1.04)	50–1.50	50–1.50
<i>R</i> <sub>work</sub> / <i>R</i> <sub>free</sub> (%)	18.9/22.0 (24.9/29.3)	14.3/14.8 (24.6/26.5)		
Rmsd for lengths (Å)	0.014			
Rmsd for angles (°)	1.2			
Number of atoms <sup>§</sup>				
Protein/Solvent	6,850 [7,858]/958 [1,456]			
Others	75 [156]			
Mean <i>B</i> -factors (Å <sup>2</sup> )				
Protein/Solvent	14.8/32.4			
Others	34.5			
Ramachandran plot (%)				
Favoured/Allowed	97.04/2.83			
Outliers	0.13			
<i>PDB ID</i>	7YW6			

Values in parentheses are for the outer shell.

<sup>‡</sup> $R_{\text{merge}} = \sum_h \sum_i |<I_h> - I_{h,i}| / \sum_h \sum_i I_{h,i}$  where *h* enumerates the unique reflections and *I* represents their symmetry-equivalent contributors.<sup>25</sup>

<sup>§</sup>H and D atoms are counted separately and indicated in the brackets.

**Table S2. Occupancy and *B*-factor values of a monooxygen species at the bridging ligand site**

	Monooxygen atom			
Occupancy	0.85	0.9	0.95	1.00
<i>B</i> -factor (Å <sup>2</sup> )	8.5	8.9	9.3	9.7

**Table S3. Cartesian coordinates for the active site complex in Ni-B**

N	2.164687	3.364583	-1.790057	N	4.606055	-1.07049	-2.08499
C	3.574919	3.587033	-1.44897	H	4.526865	-0.10875	-2.4104
C	4.457183	2.719512	-2.35867	C	3.280381	-1.35349	2.28232
O	4.006814	1.714052	-2.90096	O	3.623584	-2.00326	3.270703
C	3.859969	3.378633	0.062185	N	2.152179	-1.66747	1.574283
C	5.268248	3.706789	0.564114	C	1.317023	-2.78922	1.991591
C	6.384432	2.692137	0.155165	C	2.106911	-4.11457	1.999085
O	5.979472	1.690662	-0.5171	O	1.908976	-4.99249	2.837941
O	7.546226	2.970388	0.513634	C	0.129793	-3.03205	1.03828
H	2.083778	2.427645	-2.18901	S	-1.30036	-1.88611	1.208343
H	3.844855	4.634198	-1.68378	H	1.832604	-1.07928	0.807517
H	3.128366	4.012044	0.588905	H	0.961978	-2.64291	3.016359
H	3.621237	2.339632	0.303428	H	0.48164	-3.03157	0.004228
H	5.57781	4.71564	0.247412	H	-0.26726	-4.03098	1.229296
H	5.257484	3.741139	1.66265	N	2.928757	-4.28274	0.93497
H	1.607475	3.321214	-0.93738	C	3.552515	-5.55428	0.68422
C	0.109306	1.26998	4.599806	H	3.013574	-3.5688	0.217716
O	1.142304	1.074595	3.971452	H	2.812858	-6.36513	0.688422
N	-0.88059	2.101285	4.174125	H	4.035398	-5.50933	-0.29522
C	-0.92299	2.615479	2.823889	O	-1.95153	-1.80874	-1.75207
C	-1.78325	3.876585	2.850934	H	-1.25551	-2.43444	-2.00464
O	-2.4341	4.211887	3.844668	C	-2.27325	-4.35859	-0.63617
C	-1.50269	1.542073	1.867116	C	-4.4921	-3.05517	-1.56908
S	-1.05134	1.774178	0.099784	C	-4.05421	-3.2747	0.998426
H	-1.69716	2.286565	4.739977	N	-1.71871	-5.35877	-0.89619
H	0.100365	2.846273	2.51121	N	-5.36124	-3.24605	-2.33413
H	-1.07667	0.585755	2.173652	O	-4.69153	-3.68724	1.879331
H	-2.59048	1.472669	1.982388	Fe	-3.10118	-2.67525	-0.31938
N	-1.78764	4.579065	1.688259	Ni	-1.39895	-0.38629	-0.68586
H	-1.41073	4.103014	0.87088	H	4.307915	-5.79219	1.446688
C	-4.16576	3.727898	-2.25524	C	5.795549	3.272647	-2.79363
O	-5.21407	4.112113	-2.78024	H	6.485173	2.450389	-2.98569
N	-3.996	2.474501	-1.76085	H	5.630619	3.833124	-3.72903
C	-5.06347	1.489633	-1.83757	H	6.242302	3.949226	-2.06348
C	-6.13134	1.769147	-0.77606	C	-0.20179	0.554838	5.900466
O	-7.30016	1.474065	-0.89622	H	0.724444	0.400958	6.459909
C	-4.53176	0.050635	-1.74645	H	-0.92662	1.090183	6.525076
S	-3.69326	-0.33917	-0.15284	H	-0.61463	-0.43209	5.661318
H	-5.56513	1.606931	-2.80486	C	-2.74606	5.640148	1.483954
H	-5.36026	-0.65316	-1.85405	H	-2.95709	6.099101	2.45134
H	-3.84113	-0.14786	-2.57105	H	-2.33219	6.393146	0.804866

H	-3.1483	2.24028	-1.237	H	-3.69209	5.272212	1.061826
H	-5.75306	2.282957	0.135758	C	-2.95174	4.640239	-2.15259
N	2.601895	-2.16026	-4.46423	H	-2.11311	4.186194	-1.61775
C	2.46448	-1.37911	-3.20867	H	-2.62143	4.895657	-3.16556
C	3.54561	-1.89532	-2.23555	H	-3.24724	5.57321	-1.66162
O	3.467518	-3.00803	-1.70286	C	4.105021	-0.17465	1.781505
C	1.051559	-1.58211	-2.64374	H	3.798751	0.722354	2.333129
S	0.696229	-0.23251	-1.43656	H	5.158277	-0.36308	1.997192
H	2.624147	-0.30455	-3.37155	H	3.988425	0.027262	0.714754
H	0.326232	-1.53767	-3.46431	C	5.734859	-1.39553	-1.22442
H	1.001143	-2.57745	-2.19018	H	6.471378	-2.01191	-1.76169
H	1.953339	-1.76147	-5.14431	H	6.192048	-0.45796	-0.89499
H	3.535037	-1.98736	-4.84215	H	5.387646	-1.96801	-0.36028

**Table S4. Cartesian coordinates for the square-planer Ni complex**

N	3.015865	5.26613	-3.35382	H	2.584712	-1.55048	-2.3236
C	2.678977	5.158818	-1.92199	H	4.178609	0.315899	-4.32796
C	4.054587	5.091663	-1.26547	H	5.325199	0.883444	-3.29717
O	4.562723	4.099108	-0.78416	N	4.916298	1.124829	-0.47905
C	1.719339	4.031243	-1.54051	H	4.671432	2.075304	-0.73407
C	1.168328	4.097195	-0.10288	C	1.773061	0.757681	3.049749
C	0.507235	2.760504	0.269094	O	0.726272	0.969655	3.613573
O	-0.71344	2.683788	0.46476	N	1.885961	-0.30722	2.059383
O	1.373302	1.797123	0.31665	C	1.604762	-1.69531	2.654284
H	3.227416	4.337821	-3.71817	C	3.005468	-2.2975	2.890393
H	2.253278	6.131757	-1.63373	O	3.61039	-2.02316	3.931547
H	0.8817	4.040352	-2.24987	C	0.608374	-2.46704	1.785897
H	2.22956	3.073591	-1.67021	S	1.021173	-2.22058	0.022192
H	1.991616	4.273399	0.600012	H	2.85095	-0.32365	1.720154
H	0.440816	4.9085	0.003673	H	1.148448	-1.54016	3.631676
H	2.211842	5.606906	-3.87695	H	0.642144	-3.53431	2.029005
H	4.629516	6.038667	-1.32627	H	-0.39069	-2.09666	2.00742
C	-1.90452	-0.55342	4.578479	N	3.52139	-3.00983	1.863982
O	-1.30271	-1.32629	3.837121	H	2.998066	-3.01495	0.987509
N	-2.74259	0.412937	4.129012	O	-0.27663	-1.02034	-2.44981
C	-2.78329	0.866062	2.753487	Ni	1.091352	-0.05339	0.196832
C	-3.7615	2.049182	2.736448	C	0.993547	-3.59822	-2.58823
O	-4.64896	2.15208	3.585927	C	-1.59678	-3.3603	-3.21616
C	-3.25333	-0.24065	1.760647	C	-0.83613	-4.44364	-0.97922
S	-2.09462	-0.21532	0.323541	N	1.948054	-3.99872	-3.1349
H	-3.33644	0.932987	4.76335	N	-2.30041	-3.62376	-4.11446
H	-1.77999	1.20558	2.465921	O	-1.01586	-5.48299	-0.50259
H	-3.17092	-1.21266	2.243821	Fe	-0.52634	-2.88786	-1.71113
H	-4.28407	-0.08567	1.43021	C	5.719551	0.922613	0.711567
N	-3.62065	2.92839	1.719596	H	6.15403	1.881214	1.005532
H	-2.7498	2.943113	1.191151	H	5.134349	0.523304	1.547358
C	-4.53227	2.361042	-2.47801	H	6.525638	0.209424	0.510508
O	-5.41588	2.326635	-3.32982	C	3.052581	1.513988	3.365539
N	-4.09517	1.250461	-1.81494	H	3.777736	0.807252	3.787548
C	-4.57197	-0.08373	-2.15506	H	3.476323	1.951702	2.455675
C	-5.73035	-0.5082	-1.25122	H	2.83027	2.300397	4.088101
O	-6.0895	-1.65037	-1.08742	C	4.923226	-3.38683	1.800992
C	-3.45078	-1.11828	-2.31174	H	5.374382	-3.18272	2.773329
S	-2.71176	-1.88173	-0.79185	H	5.023241	-4.45281	1.569756
H	-5.03366	0.025116	-3.14973	H	5.424949	-2.80356	1.021941
H	-3.80844	-1.99443	-2.85569	C	-1.69876	-0.57646	6.073557

H	-2.61876	-0.69512	-2.87751	H	-0.78556	-0.01143	6.294247
H	-3.32823	1.314649	-1.15493	H	-2.5245	-0.12579	6.634947
H	-6.2572	0.346398	-0.76773	H	-1.5485	-1.60579	6.407697
N	4.586594	0.190037	-3.40367	C	-3.85749	3.668255	-2.07855
C	3.55428	0.394739	-2.37067	H	-4.59834	4.318654	-1.60214
C	4.243926	0.075005	-1.02723	H	-3.00166	3.535992	-1.409
O	4.284364	-1.04732	-0.53117	H	-3.52303	4.172123	-2.99045
C	2.375691	-0.53352	-2.65934	C	-4.57325	4.02576	1.617419
S	0.773516	0.064381	-1.95031	H	-4.58318	4.628717	2.532549
H	3.199557	1.441429	-2.33527	H	-4.2938	4.655804	0.771358
H	2.174274	-0.57652	-3.73492	H	-5.5842	3.638184	1.459277

**Table S5. Comparison of the selected bond lengths (Å) of the proximal [4Fe-4S] cluster in the oxidized and reduced enzymes**

	Oxidized	Reduced <sup>‡</sup>	$\Delta$
N (Gly19 <sup>S</sup> )–S $\gamma$ (Cys17 <sup>S</sup> )	3.25	3.25	0
Fe1–S $\gamma$ (Cys17 <sup>S</sup> )	2.28	2.28	0
Fe1–S2	2.29	2.34	–0.05
Fe1–S3	2.28	2.34	–0.06
Fe1–S4	2.20	2.24	–0.04
Fe2–S $\gamma$ (Cys114 <sup>S</sup> )	2.28	2.28	0
Fe2–S1	2.29	2.32	–0.03
Fe2–S3	2.22	2.28	–0.06
Fe2–S4	2.26	2.29	–0.03
Fe3–S $\gamma$ (Cys150 <sup>S</sup> )	2.26	2.29	–0.03
Fe3–S1	2.28	2.32	–0.04
Fe3–S2	2.24	2.28	–0.04
Fe3–S4	2.30	2.34	–0.04
Fe4–S $\gamma$ (Cys20 <sup>S</sup> )	2.24	2.26	–0.02
Fe4–S1	2.20	2.27	–0.07
Fe4–S2	2.29	2.32	–0.03
Fe4–S3	2.28	2.34	–0.06

<sup>‡</sup>The values are derived from the high-resolution X-ray structure determined previously (PDB ID: 4U9H).<sup>19</sup>

**Table S6. Comparison of the selected bond lengths (Å) of the medial [3Fe-4S] cluster in the oxidized and reduced enzymes**

	Oxidized	Reduced <sup>‡</sup>	$\Delta$
Fe1–S $\gamma$ (Cys249 <sup>S</sup> )	2.32	2.33	–0.01
Fe1–S1	2.23	2.23	0
Fe1–S2	2.26	2.30	–0.04
Fe1–S3	2.28	2.31	–0.03
Fe3–S $\gamma$ (Cys231 <sup>S</sup> )	2.29	2.30	–0.01
Fe3–S1	2.22	2.23	–0.01
Fe3–S3	2.32	2.30	+0.02
Fe3–S4	2.28	2.29	–0.01
Fe4–S $\gamma$ (Cys252 <sup>S</sup> )	2.33	2.32	+0.01
Fe4–S2	2.26	2.26	0
Fe4–S3	2.30	2.32	–0.02
Fe4–S4	2.23	2.26	–0.03

<sup>‡</sup>The values are derived from the high-resolution X-ray structure determined previously (PDB ID: 4U9H).<sup>19</sup>

**Table S7. Comparison of the selected bond lengths (Å) of the distal [4Fe-4S] cluster in the oxidized and reduced enzymes**

	Oxidized	Reduced <sup>‡</sup>	$\Delta$
Fe1–N $\delta$ 1 (His188 <sup>S</sup> )	2.03	2.07	–0.04
Fe1–S2	2.25	2.33	–0.08
Fe1–S3	2.23	2.29	–0.06
Fe1–S4	2.28	2.31	–0.03
Fe2–S $\gamma$ (Cys222 <sup>S</sup> )	2.31	2.32	–0.01
Fe2–S1	2.24	2.35	–0.09
Fe2–S3	2.28	2.31	–0.03
Fe2–S4	2.22	2.29	–0.07
Fe3–S $\gamma$ (Cys191 <sup>S</sup> )	2.30	2.32	–0.02
Fe3–S1	2.19	2.30	–0.11
Fe3–S2	2.24	2.32	–0.08
Fe3–S4	2.25	2.34	–0.09
Fe4–S $\gamma$ (Cys216 <sup>S</sup> )	2.28	2.29	–0.01
Fe4–S1	2.27	2.32	–0.05
Fe4–S2	2.21	2.27	–0.06
Fe4–S3	2.26	2.34	–0.08

<sup>‡</sup>The values are derived from the high-resolution X-ray structure determined previously (PDB ID: 4U9H).<sup>19</sup>

## ESI References

1. N. Yahata, T. Saitoh, Y. Takayama, K. Ozawa, H. Ogata, Y. Higuchi and H. Akutsu, *Biochemistry*, 2006, **45**, 1653–1662.
2. Y. Higuchi, N. Yasuoka, M. Kakudo, Y. Katsube, T. Yagi and H. Inokuchi, *J. Biol. Chem.*, 1987, **262**, 2823–2825.
3. T. Hiromoto, K. Nishikawa, T. Tamada and Y. Higuchi, *Top. Catal.*, 2021, **64**, 622–630.
4. T. Nakamura, M. Katagiri, T. Hosoya, K. Toh, M. Kitaguchi, M. Hino, T. Ebisawa, K. Sakasai and K. Soyama, *IEEE Nucl. Sci. Symp. Med. Imaging Conf. Rec. (NSS/MIC)*, 2012, 222–225.
5. I. Tanaka, K. Kusaka, T. Hosoya, N. Niimura, T. Ohhara, K. Kurihara, T. Yamada, Y. Ohnishi, K. Tomoyori and T. Yokoyama, *Acta Crystallogr., Sect. D: Biol. Crystallogr.*, 2010, **66**, 1194–1197.
6. K. Kusaka, T. Hosoya, T. Yamada, K. Tomoyori, T. Ohhara, M. Katagiri, K. Kurihara, I. Tanaka and N. Niimura, *J. Synchrotron Rad.*, 2013, **20**, 994–998.
7. T. Ohhara, K. Kusaka, T. Hosoya, K. Kurihara, K. Tomoyori, N. Niimura, I. Tanaka, J. Suzuki, T. Nakatani, T. Otomo, S. Matsuoka, K. Tomita, Y. Nishimaki, T. Ajima and S. Ryufuku, *Nucl. Instrum. Methods Phys. Res., Sect. A*, 2009, **600**, 195–197.
8. N. Yano, T. Yamada, T. Hosoya, T. Ohhara, I. Tanaka, N. Niimura and K. Kusaka, *Acta Crystallogr., Sect. D: Biol. Crystallogr.*, 2018, **74**, 1041–1052.
9. P. V. Afonine, M. Mustyakimov, R. W. Grosse-Kunstleve, N. W. Moriarty, P. Langan and P. D. Adams, *Acta Crystallogr., Sect. D: Biol. Crystallogr.*, 2010, **66**, 1153–1163.
10. W. Kabsch, *Acta Crystallogr., Sect. D: Biol. Crystallogr.*, 2010, **66**, 125–132.
11. A. J. McCoy, R. W. Grosse-Kunstleve, P. D. Adams, M. D. Winn, L. C. Storoni and R. J. Read, *J. Appl. Cryst.*, 2007, **40**, 658–674.
12. P. D. Adams, P. V. Afonine, G. Bunkóczi, V. B. Chen, I. W. Davis, N. Echols, J. J. Headd, L. Hung, G. J. Kapral, R. W. Grosse-Kunstleve, A. J. McCoy, N. W. Moriarty, R. Oeffner, R. J. Read, D. C. Richardson, J. S. Richardson, T. C. Terwilliger and P. H. Zwart, *Acta Crystallogr., Sect. D: Biol. Crystallogr.*, 2010, **66**, 213–221.
13. P. Emsley, B. Lohkamp, W. G. Scott and K. Cowtan, *Acta Crystallogr., Sect. D: Biol. Crystallogr.*, 2010, **66**, 486–501.
14. J. Bergmann, E. Oksanen and U. Ryde, *Curr. Opin. Struct. Biol.*, 2022, **72**, 18–26.
15. A. D. Becke, *J. Chem. Phys.*, 1993, **98**, 5648–5652.
16. P. C. Hariharan and J. A. Pople, *Theor. Chim. Acta*, 1973, **28**, 213–222.
17. V. A. Rassolov, J. A. Pople, M. A. Ratner and T. L. Windus, *J. Chem. Phys.*, 1998, **109**, 1223–1229.
18. M. J. Frisch, G. W. Trucks, H. B. Schlegel, G. E. Scuseria, M. A. Robb, J. R. Cheeseman, G. Scalmani, V. Barone, G. A. Petersson, H. Nakatsuji, X. Li, M. Caricato, A. V. Marenich, J. Bloino, B. G. Janesko, R. Gomperts, B. Mennucci, H. P. Hratchian, J. V. Ortiz, A. F. Izmaylov, J. L. Sonnenberg, D. Williams-Young, F. Ding, F. Lipparini, F. Egidi, J. Goings, B. Peng, A. Petrone, T. Henderson, D. Ranasinghe, V. G. Zakrzewski, J. Gao, N. Rega, G. Zheng, W. Liang, M. Hada, M. Ehara, K. Toyota, R. Fukuda, J. Hasegawa, M. Ishida, T. Nakajima, Y. Honda, O. Kitao, H. Nakai, T. Vreven, K. Throssell, J. A. Montgomery, Jr., J. E. Peralta, F. Ogliaro, M. J. Bearpark, J. J. Heyd, E. N. Brothers, K. N. Kudin, V. N. Staroverov, T. A. Keith, R. Kobayashi, J. Normand, K. Raghavachari, A. P. Rendell, J. C. Burant, S. S. Iyengar, J. Tomasi, M. Cossi, J. M. Millam, M. Klene, C. Adamo, R. Cammi, J. W. Ochterski, R. L. Martin, K. Morokuma, O. Farkas, J. B. Foresman and D. J. Fox, in *Gaussian 16, Revision C.01*, Gaussian, Inc., Wallingford CT, USA, 2016.
19. H. Ogata, K. Nishikawa and W. Lubitz, *Nature*, 2015, **520**, 571–574.
20. I. Fdez. Galván, A. Volbeda, J. C. Fontecilla-Camps and M. J. Field, *Proteins*, 2008, **73**, 195–203.
21. H. Ishikita and K. Saito, *J. R. Soc. Interface*, 2014, **11**, 20130518.
22. A. Volbeda, M. H. Charon, C. Piras, E. C. Hatchikian, M. Frey and J. C. Fontecilla-Camps, *Nature*, 1995, **373**, 580–587.
23. K. Takeda and K. Miki, *FEBS J.*, 2017, **284**, 2163–2166.

24. M. E. Pandelia, D. Bykov, R. Izsak, P. Infossi, M. T. Giudici-Ortoni, E. Bill, F. Neese and W. Lubitz, *Proc. Natl. Acad. Sci. U.S.A.*, 2013, **110**, 483–488.
25. A. Wlodawer, W. Minor, Z. Dauter and M. Jaskolski, *FEBS J.*, 2013, **280**, 5705–5736.